Dissolution of a vertical solid surface by turbulent compositional convection

Ross C. Kerr[1],† and Craig D. McConnochie[1]

[1]Research School of Earth Sciences, The Australian National University, Canberra, ACT 0200, Australia

We examine the dissolution of a vertical solid surface in the case where the heat and mass transfer is driven by turbulent compositional convection. A theoretical model of the turbulent dissolution of a vertical wall is developed, which builds on the scaling analysis presented by Kerr (*J. Fluid Mech.*, vol. 280, 1994, pp. 287–302) for the turbulent dissolution of a horizontal floor or roof. The model has no free parameters and no dependence on height. The analysis is tested by comparing it with laboratory measurements of the ablation of a vertical ice wall in contact with salty water. The model is found to accurately predict the dissolution velocity for water temperatures up to approximately 5–6 °C, where there is a transition from turbulent dissolution to turbulent melting. We quantify the turbulent convective dissolution of vertical ice bodies in the polar oceans, and compare our results with some field observations.

Key words: phase change, solidification/melting, turbulent convection

---

1. Introduction

Over the past decade, an important component of global climate change has been the increasingly rapid decrease in the mass of the Antarctic and Greenland Ice Sheets (Rignot *et al.* 2011). This ongoing mass loss is occurring on the underside and fronts of ice shelves formed where glaciers reach the polar oceans (Jenkins *et al.* 2010) and from the icebergs that calve from them (Budd, Jacka & Morgan 1980). Around Antarctica, Rignot *et al.* (2013) estimate that approximately 55 % of the annual mass loss (1500 Gt yr^{-1}) is from ice shelves and approximately 45 % (1265 Gt yr^{-1}) is from calved icebergs. Field observations of both icebergs and ice shelves indicate that this mass loss is an increasing function of ocean temperature (e.g. Budd *et al.* 1980; Shepherd, Wingham & Rignot 2004).

Depending on the temperature of the seawater, icebergs and floating ice shelves may either melt or dissolve. Melting will occur when the seawater is sufficiently warm, and it is controlled only by heat transfer (Woods 1992; Kerr 1994*a*). During melting, the interface salinity is zero, and the interface temperature is the melting point of ice (e.g. 0 °C at atmospheric pressure). In contrast, dissolving will occur when the sea is close to or below the melting point of ice, and it is controlled by a combination of heat and mass transfer (Woods 1992; Kerr 1994*b*). During dissolving, the interface salinity is non-zero, and the interface temperature is less than the melting point of ice.

† Email address for correspondence: ross.kerr@anu.edu.au

In a recent study, Wells & Worster (2011) quantified the melting and dissolving of a vertical solid surface driven by laminar compositional convection. They analysed the structure of the thermal and compositional boundary layers during both melting and dissolving, and determined the condition for the transition between the melting and dissolving regimes. However, this analysis cannot be used to predict the melting and dissolving of large bodies of ice in the polar oceans, because the convective flow becomes turbulent after a vertical distance of 10–20 cm (Josberger & Martin 1981; Carey & Gebhart 1982; Johnson & Mollendorf 1984), while icebergs have vertical heights of 100 m in the North Atlantic Ocean and 250 m in the Southern Ocean.

In this paper, we aim to quantify the turbulent dissolution of a vertical ice wall. In § 2, we present a theoretical model of dissolution by turbulent compositional convection of a vertical solid surface. In § 3, the model is compared with experimental observations of vertical ice walls ablating in water at oceanic salinities, made by Josberger & Martin (1981) and by ourselves. In § 4, we quantify the turbulent convective dissolution of vertical ice bodies in the polar oceans. Our conclusions are given in § 5.

2. Dissolving theory

In this section, we examine turbulent thermal convection on vertical and horizontal boundaries in § 2.1, before the dissolution of a vertical solid surface by turbulent compositional convection is considered in § 2.2.

2.1. *Turbulent thermal convection*

In understanding mass transfer due to turbulent compositional convection, very useful insight can be gained by examining the experimental measurements on turbulent heat transfer by natural convection tabulated by Holman (2010).

For turbulent natural convection on an isothermal vertical boundary of temperature T_w, the expression for the Nusselt number Nu at high Rayleigh numbers Ra is given by

$$Nu = 0.10 \, Ra^{1/3} \tag{2.1}$$

(Holman 2010, p. 335), where $Nu = qH(k(T_w - T_f))^{-1}$, q is the heat flux from the boundary, H is the height of the boundary, k is the thermal conductivity of the fluid, T_f is the far-field temperature of the fluid, $Ra = g\alpha(T_w - T_f)H^3(\kappa\nu)^{-1}$, g is the gravitational acceleration, α is the thermal expansion coefficient of the fluid, κ is the thermal diffusivity of the fluid, and ν is the kinematic viscosity of the fluid. Equation (2.1) was measured in air by Warner & Arpaci (1968) using a 3.7 m high plate, for Rayleigh numbers that ranged from 10^9 up to 10^{12}.

For turbulent natural convection on a constant-heat-flux vertical boundary, the Nusselt number at high flux Rayleigh numbers Ra_f is given by

$$Nu = 0.17 \, Ra_f^{1/4} \tag{2.2}$$

(Holman 2010, p. 336), where $Ra_f = g\alpha qH^4(k\kappa\nu)^{-1}$. Equation (2.2) was measured in air by Vliet & Ross (1975) using a 7.3 m high plate, for flux Rayleigh numbers that ranged from 2×10^{13} up to 10^{16}. Since $Ra_f = Ra \, Nu$, we note that (2.2) is equivalent to

$$Nu = (0.17)^{4/3} \, Ra^{1/3} = 0.094 \, Ra^{1/3}, \tag{2.3}$$
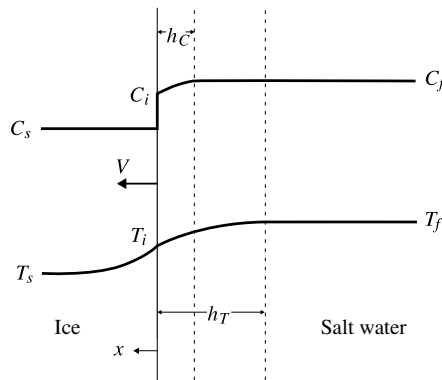
FIGURE 1. The thermal and compositional profiles when ice dissolves into salt water at velocity V. The thermal boundary layer has a thickness h_T and the compositional boundary layer has a thickness h_C.

for Rayleigh numbers that range from 5×10^{10} to 6×10^{12}, which demonstrates that the turbulent heat transfer expressions (2.1) and (2.2) are in very good agreement.

For turbulent natural convection from a horizontal boundary, the Nusselt number at high Rayleigh numbers is given by

$$Nu = 0.156\,Ra^{1/3}, \tag{2.4}$$

where H here is the height of the fluid layer. Equation (2.4) was measured in 0.45 m high water by Katsaros *et al.* (1977), for Rayleigh numbers from 3×10^8 to 4×10^9.

It is important to note that (2.1), (2.3) and (2.4) show that a one-third power law dependence on Rayleigh number applies equally as well for turbulent natural convection at both horizontal and vertical boundaries. For a horizontal boundary, the one-third power law dependence implies that the turbulent heat flux is independent of the height of the fluid (cf. Turner 1979, p. 213). For a vertical boundary, the one-third power law dependence implies that the turbulent heat flux is independent of the height of the boundary and independent of position on the vertical boundary (cf. Holman 2010, p. 337).

2.2. *Dissolution of a vertical solid surface by turbulent compositional convection*

Consider the turbulent dissolution at velocity V of a vertical solid surface of composition C_s, melting temperature T_m and far-field temperature T_s, in contact with a semi-infinite fluid with a far-field composition C_f and a far-field temperature T_f. The resulting thermal and compositional profiles are shown in figure 1 (cf. figure 1(*b*) of Wells & Worster 2011) and illustrated on a typical phase diagram in figure 2. At the interface between the solid and the fluid, the temperature T_i and composition C_i are constrained thermodynamically to lie on the liquidus curve

$$T_i = T_L(C_i), \tag{2.5}$$

which gives the freezing temperature of the fluid as a function of concentration. Within the solid, the balance between thermal diffusion and ablation results in a temperature given by

$$T(x) = T_s + (T_i - T_s)\mathrm{e}^{-x/h_s} \tag{2.6}$$
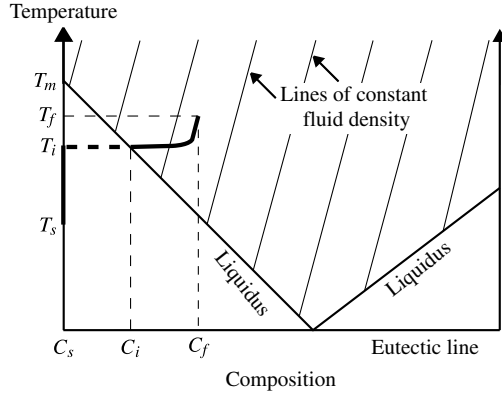
FIGURE 2. The path on a simple phase diagram of the thermal and compositional profiles shown in figure 1. The dashed portion of the path represents the jump in composition at the dissolving interface.

(Carslaw & Jaeger 1986), where the length scale $h_s = \kappa_s/V$, and κ_s is the thermal diffusivity of the solid.

There are compositional and thermal boundary layers immediately adjacent to the interface. If the respective turbulent fluxes to the interface through these layers are F_C and F_T, the effective layer thicknesses h_C and h_T can be defined by

$$F_C = \frac{D(C_f - C_i)}{h_C} \tag{2.7}$$

and

$$F_T = \frac{k_f(T_f - T_i)}{h_T}, \tag{2.8}$$

where D and k_f are the compositional diffusivity and thermal conductivity of the fluid. For simplicity, we neglect the volume change associated with the phase change (cf. Woods 1992), which for ice is approximately 8 %. The boundary layer fluxes are linked to the dissolving velocity V by the interfacial conditions

$$F_C = V(C_i - C_s) \tag{2.9}$$

and

$$F_T = V(\rho_s L_s + \rho_s c_s(T_i - T_s)), \tag{2.10}$$

where ρ_s, L_s and c_s are the density, latent heat and specific heat of the solid. Equations (2.9) and (2.10) represent conservation of composition and conservation of heat at the interface.

The interface between the solid and the fluid is assumed to be flat, and the compositional buoyancy released at the interface is assumed to dominate the thermal buoyancy, i.e. that the ratio $\mathscr{R}$ of these buoyancies satisfies the condition

$$\mathscr{R} \equiv \frac{\beta(C_f - C_s)}{\alpha[\rho_s L_s + \rho_s c_s(T_i - T_s)]/\rho_f c_f} \gg 1, \tag{2.11}$$

where α is the coefficient of thermal expansion and β is the equivalent coefficient for the variation of density with composition (cf. Kerr 1994*a,b*).

Following Kerr (1994*b*), it is envisaged that both the compositional and thermal boundary layers grow diffusively with time t:

$$h_C \sim \sqrt{Dt} \tag{2.12}$$

and

$$h_T \sim \sqrt{\kappa_f t}, \tag{2.13}$$

where c_f and $\kappa_f \equiv k_f/\rho_f c_f$ are the specific heat and thermal diffusivity of the fluid, until a typical time τ when they are periodically removed by the eddies associated with the turbulent buoyant compositional convection (cf. Lick 1965; Howard 1966). From the empirical expressions (2.1) and (2.3) for turbulent heat transfer from a vertical boundary given in §2.1, the mass transfer due to turbulent compositional convection is expected to be given by

$$Nu = \gamma \, Ra^{1/3}, \tag{2.14}$$

where the constant γ has a value of approximately 0.097 ± 0.010. Equation (2.14) corresponds to a compositional boundary layer thickness

$$h_C = \frac{1}{\gamma} \left(\frac{D\mu}{g(\rho_f - \rho_i)} \right)^{1/3}, \tag{2.15}$$

where g is the acceleration due to gravity, ρ_f is the density of the far-field fluid, ρ_i is the density of the fluid at the interface, and μ is the fluid viscosity. Combining (2.15), (2.12) and (2.13) gives

$$h_T = h_C \left(\frac{\kappa_f}{D} \right)^{1/2} = \frac{1}{\gamma} \left(\frac{\mu^2 \kappa_f^3}{Dg^2(\rho_f - \rho_i)^2} \right)^{1/6} \tag{2.16}$$

and

$$\tau \approx \frac{1}{\gamma^2} \left(\frac{\mu^2}{Dg^2(\rho_f - \rho_i)^2} \right)^{1/3}. \tag{2.17}$$

Substitution of (2.15) and (2.7) into (2.9) then yields the prediction that the dissolving velocity

$$V = \gamma \left(\frac{g(\rho_f - \rho_i)D^2}{\mu} \right)^{1/3} \left(\frac{C_f - C_i}{C_i - C_s} \right), \tag{2.18}$$

while combining (2.18), (2.16), (2.8), (2.10) and (2.5) shows that

$$T_f - T_L(C_i) = \frac{\rho_s L_s + \rho_s c_s (T_L(C_i) - T_s)}{\rho_f c_f} \left(\frac{D}{\kappa_f} \right)^{1/2} \left(\frac{C_f - C_i}{C_i - C_s} \right). \tag{2.19}$$

In the above analysis, it has been implicitly assumed that the distance $\sqrt{D\tau}$ over which compositional diffusion occurs is large in comparison with the distance $V\tau$ that the solid has dissolved in the convective timescale τ. From (2.15), (2.17) and (2.18), it is found that

$$V\tau \approx \frac{h_C}{\mathscr{C}}, \tag{2.20}$$

where

$$\mathscr{C} \equiv \frac{C_i - C_s}{C_f - C_i}. \tag{2.21}$$

Equations (2.18) and (2.19) are therefore asymptotically correct when $\mathscr{C} \gg 1$. However, if $\mathscr{C}$ is smaller (i.e. $\mathscr{C} \sim 1$), then (2.20) suggests that h_C is more accurately estimated by

$$h_C = \sqrt{D\tau} + V\tau = \frac{1}{\gamma} \left(\frac{D\mu}{g(\rho_f - \rho_i)} \right)^{1/3} \left(1 + \frac{1}{\mathscr{C}} \right), \tag{2.22}$$

which results in V and $T_f - T_i$ being given by

$$V = \gamma \left(\frac{g(\rho_f - \rho_i)D^2}{\mu} \right)^{1/3} \left(\frac{C_f - C_i}{C_f - C_s} \right), \tag{2.23}$$

and

$$T_f - T_L(C_i) = \frac{\rho_s L_s + \rho_s c_s (T_L(C_i) - T_s)}{\rho_f c_f} \left(\frac{D}{\kappa_f} \right)^{1/2} \left(\frac{C_f - C_i}{C_f - C_s} \right). \tag{2.24}$$

It is then concluded that the dissolving rate is given by (2.23), once C_i is evaluated from (2.24). We also note that when when $\mathscr{C} \ll 1$, $\sqrt{D\tau} \ll V\tau$, and the above scaling analysis breaks down, as the turbulent dissolving undergoes a transition to turbulent melting (see the Appendix of Kerr 1994*b*).

3. Comparison with laboratory experiments

3.1. *The experiments of Josberger & Martin (1981)*

Josberger & Martin (1981) conducted a careful series of experiments in which a vertical ice wall ablated in contact with homogeneous aqueous solutions of sodium chloride. The ice was bubble-free, up to 1.2 m high, and had an initial temperature of $-1\,°$C. The solutions had compositions C_f from 2.90 to 3.52 wt% NaCl, and temperatures T_f that ranged from 0 to 27 °C. For solution temperatures up to 20 °C, the convective flow on the lower part of the ice wall consisted of a laminar upflow inside an outer laminar downflow (figure 3). However, at a height of 10–30 cm from the base of the ice wall, there was a transition to a turbulent upflow. The upflow was observed to grow in thickness and velocity with height, and its outer edge was seen to fluctuate with the passage of turbulent eddies.

The turbulent flow data from the nine experiments of Josberger & Martin (1981) are summarized in table 1. The table lists the temperature T_f and composition C_f of the sodium chloride solutions, the measured interface temperature T_w, and the ablation velocities V measured at various vertical distances z above the height on the ice wall at which the upward flow became turbulent. The interface temperatures were found to be constant to within $0.02\,°$C along the ice in each experiment. The ablation velocities are also reasonably constant, to within approximately 5–10 %. We note that Josberger & Martin (1981) attempted to understand their ablation results using a $V \propto z^{-1/4}$ power law, but this scaling law does not fit all their data well (i.e. it gives a variation with z of 23 % for experiment 4, and a variation of 20 % for experiment 5; see their table 3), and it should only be relevant to ablation by laminar flow (see Wells & Worster 2011).

When the turbulent dissolution model in §2.2 is compared with the turbulent ablation experiments of Josberger & Martin (1981), it can only be applied to experiments 1–6, as these are the only experiments that are in the dissolving regime. The turbulent flow in these experiments covers vertical length scales of approximately
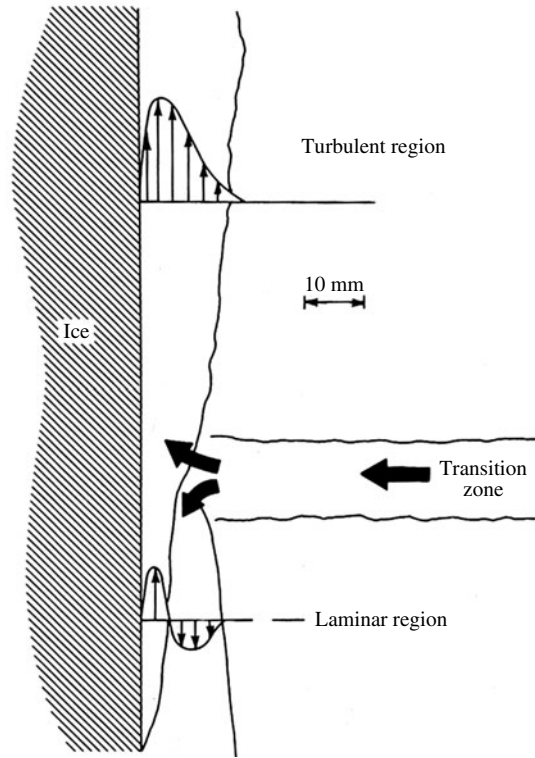
FIGURE 3. Sketch by Josberger & Martin (1981) of the convective flows beside the ice wall, for $T_f < 20\,°C$ and $C_f = 2.90$–3.52 wt% NaCl.

0.1–1 m, and Rayleigh numbers of approximately 10^{10}–10^{14}. The corresponding model predictions are listed in table 2. The predicted interface temperatures T_i, which are determined from (2.5) and (2.24), agree with the measured interface temperatures T_w of Josberger & Martin (1981) to within $0.1\,°C$ (see figure 4). We note that (2.24) is only expected to be accurate for $\mathscr{C} \sim 1$ or greater, but $\mathscr{C}$ is only 0.38 in experiment 6.

In figure 5, the measured dissolving velocities V of Josberger & Martin (1981) are plotted against the predicted velocity scale

$$\mathscr{V} = \left(\frac{g(\rho_f - \rho_i)D^2}{\mu_f} \right)^{1/3} \left(\frac{C_f - C_i}{C_f - C_s} \right) \tag{3.1}$$

from (2.23). The dissolving velocities are seen to lie on a straight line, whose slope $\gamma = 0.093 \pm 0.010$ is consistent with the value of approximately 0.097 ± 0.010 predicted from the turbulent heat transfer expressions (2.1) and (2.3) in § 2.1.

In experiments 7–9 of Josberger & Martin (1981), the fluid temperature T_f is too high to allow a solution for C_i in (2.24). Experiment 7 lies in the transition regime between dissolution and melting (cf. the Appendix to Kerr 1994*b*), while in experiments 8 and 9, the interface temperatures are so close to $0\,°C$ (see table 1) that these two experiments can be viewed as being in the regime of turbulent melting (cf. Kerr 1994*a*, and figure 10 of Josberger & Martin 1981).
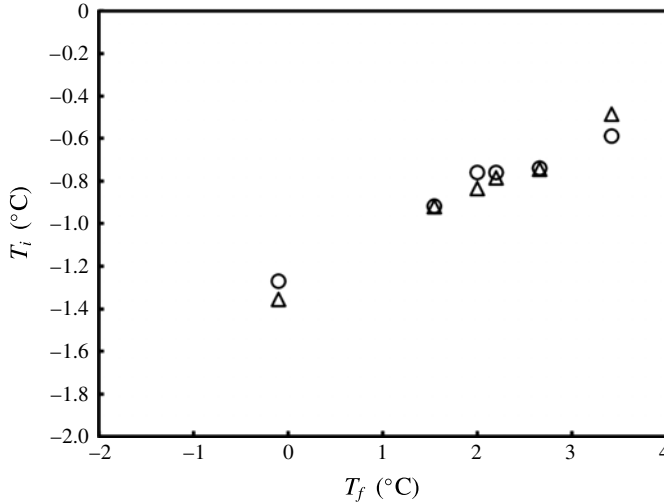
FIGURE 4. A comparison of the predicted interface temperature T_i ($\triangle$) with the measured interface temperature T_w ($\bigcirc$) of Josberger & Martin (1981), plotted as a function of the temperature T_f of the NaCl solution. The experiments have a range in C_f from 2.90 to 3.44 wt% NaCl.

Experiment number	T_f (°C)	C_f (wt%)	T_w (°C)	z (mm)	V (μm s^{-1})
1	−0.10	2.99	−1.27	360	0.58
2	1.55	2.90	−0.92	70	1.22
				200	1.02
3	2.00	3.00	−0.76	510	1.57
				610	1.56
				940	1.40
4	2.20	3.00	−0.76	115	1.87
				250	1.89
5	2.66	3.44	−0.74	180	2.15
				330	2.33
6	3.42	3.00	−0.59	470	2.47
				520	2.23
7	6.85	3.395	−0.20	220	6.29
				360	5.99
8	10.85	3.41	−0.06	240	9.58
				370	9.16
9	16.31	3.52	−0.02	290	14.27

TABLE 1. The turbulent ablation results of Josberger & Martin (1981) and Josberger (1979). Note that T_w for experiment 7 is taken from Josberger (1979), as it is incorrectly given in Josberger & Martin (1981).

3.2. *Our experiments*

In addition to Josberger & Martin (1981), some ice ablation experiments were reported by Russell-Head (1980) and Johnson & Mollendorf (1984). However, the ice
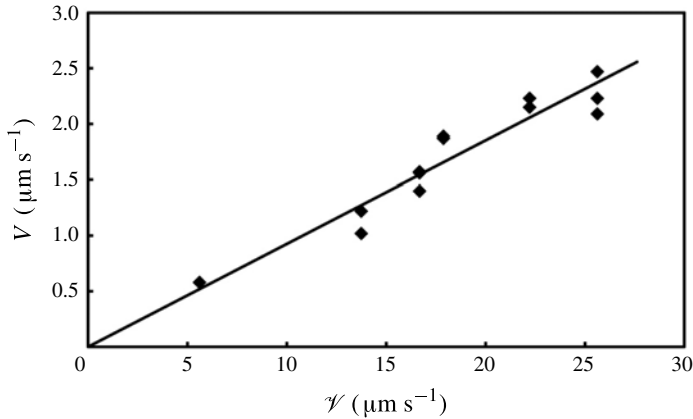
FIGURE 5. The dissolving velocities V of Josberger & Martin (1981), in comparison with the velocity scale $\mathscr{V}$ defined by (3.1). The values lie on a straight line with a constant of proportionality of 0.093 ± 0.010.

Quantity	1	2	3	4	5	6	Units
T_f	−0.10	1.55	2.00	2.20	2.66	3.42	K
C_f	2.99	2.90	3.00	3.00	3.44	3.00	wt%
ρ_f	1022.7	1021.9	1022.6	1022.6	1025.9	1022.6	kg m^{-3}
c_f	4.03	4.04	4.03	4.03	4.01	4.03	J g^{-1} K^{-1}
k_f	0.554	0.557	0.557	0.557	0.557	0.559	W m^{-1} K^{-1}
ν	1.85	1.83	1.82	1.82	1.82	1.80	mm^2 s^{-1}
C_i	2.28	1.56	1.41	1.32	1.25	0.82	wt%
T_i	−1.36	−0.92	−0.83	−0.79	−0.74	−0.48	K
ρ_i	1017.3	1011.7	1010.6	1009.9	1009.4	1006.0	kg m^{-3}
$\mathscr{C}$	3.22	1.16	0.89	0.79	0.58	0.38	
$\mathscr{V}$	5.6	13.7	16.7	17.9	22.2	25.7	μm s^{-1}

TABLE 2. Experimental parameters (ρ_f, c_f, k_f, μ) and theoretical predictions (C_i, T_i, ρ_i, $\mathscr{C}$, $\mathscr{V}$) for experiments 1–6 of Josberger & Martin (1981) listed in table 1. The physical properties of the aqueous NaCl solutions were obtained from data in Washburn (1926), Weast (1989) and Batchelor (1967). Other parameters used are $\rho_s L_s = 306$ J cm^{-3} (Washburn 1926), $\rho_s c_s = 1.832$ J cm^{-3} K^{-1} (Weast 1989), and the expression $D = 10^{-5.144 + 0.0127 T_i}$ cm^2 s^{-1}, where T_i has units of K, which was inferred from data in Washburn (1926) that is accurate to approximately 3%. Consistent with the compositional and thermal profiles sketched in figure 1, the parameter ν is evaluated at $(C_f + C_i)/2$ and T_i, while k_f is evaluated at C_f and $(T_i + T_f)/2$.

was only 20–30 cm high in both studies. This small scale resulted in mostly laminar compositional convection, and ablation that varied significantly with height, so their results are not analysed here. Instead, we conducted our own ice ablation experiments, in a temperature controlled room set at approximately 4 °C. Our experiments used a rectangular tank that was 1.2 m high, 0.2 m wide and 1.5 m long. To limit heat transfer, the sidewalls of the tank consisted of an inner sheet of 20 mm thick acrylic and an outer sheet of 2 mm thick acrylic, separated by an 18 mm gap filled with

Quantity	A	B	C	D	E	F	G	H	Units
T_f	0.3	1.3	2.3	3.1	3.8	4.2	4.7	5.4	K
C_f	3.44	3.49	3.50	3.47	3.46	3.60	3.60	3.49	wt%
T_w	−1.31	−1.01	−0.76	−0.62	−0.53	−0.55	−0.43	−0.35	K
V	0.7	1.1	1.7	2.3	2.6	3.0	3.0	3.4	μm s^{-1}
dT/dt	0.0006	0.0012	0.0016	0.0011	0.0024	0.0044	0.0048	0.0077	K min^{-1}
$T_i - T_s$	24	20	11	4	7	10	11	13	K
ρ_f	1026.1	1026.4	1026.4	1026.1	1026.0	1027.0	1027.0	1026.1	kg m^{-3}
c_f	4.01	4.00	4.00	4.01	4.01	4.00	4.00	4.00	J g^{-1} K^{-1}
k_f	0.554	0.555	0.557	0.558	0.559	0.559	0.559	0.560	W m^{-1} K^{-1}
ν	1.85	1.84	1.82	1.80	1.79	1.78	1.78	1.78	mm^2 s^{-1}
C_i	2.45	2.03	1.53	1.10	0.81	0.69	0.47	0.19	wt%
T_i	−1.45	−1.20	−0.91	−0.65	−0.48	−0.41	−0.28	−0.11	K
ρ_i	1018.5	1015.3	1011.5	1008.2	1006.1	1005.1	1003.4	1001.3	kg m^{-3}
$\mathscr{C}$	2.48	1.38	0.78	0.46	0.31	0.24	0.15	0.06	
$\mathscr{V}$	7.6	12.7	18.9	24.6	28.7	31.5	34.7	38.7	μm s^{-1}

TABLE 3. Experimental parameters, and theoretical predictions (C_i, T_i, ρ_i, $\mathscr{C}$, $\mathscr{V}$), for our eight ice ablation experiments (A–H). The physical properties of the aqueous NaCl solutions were calculated as described in table 2. Other parameters used are $\rho_s L_s = 306$ J cm^{-3} (Washburn 1926), $\rho_s c_s = 1.832$ J cm^{-3} K^{-1} (Weast 1989), and the expression $D = 10^{-5.144+0.0127 T_i}$ cm^2 s^{-1}, where T_i has units of K, which was inferred from data in Washburn (1926) that is accurate to approximately 3 %. From the measured temperature rise dT/dt in the ice near the interface, (3.2) was used to evaluate the equivalent temperature difference $T_i - T_s$ of a semi-infinite block of ice.

argon gas. One endwall of the tank consisted of an aluminium heat exchanger, through which ethanol was circulated from a Julabo FP50 Refrigerated–Heating Circulator.

To grow the ice, the tank was first filled with cold fresh water and the circulator was set to approximately −10 °C. An aquarium air pump was then used to supply a rising stream of air bubbles near the cold wall, which ensured that the growing ice was bubble-free.

Once the ice wall was approximately 8 cm thick, the circulator was reset to approximately −2 °C to allow the ice to equilibrate to a uniform temperature T_s close to the anticipated interface temperature T_i. The cold fresh water was then pumped out of the tank, and replaced by homogeneous aqueous solutions of sodium chloride. The solutions had compositions C_f from 3.44 to 3.60 wt% NaCl, and temperatures T_f that ranged from 0.3 to 5.4 °C (table 3). Experiments E–H were performed to investigate the transition from dissolving to melting, and had temperatures between experiments 6 and 7 of Josberger & Martin (1981).

The experiments were viewed using the shadowgraph method, and recorded with regular photographs from a digital camera. The photographs showed a laminar flow in the lower 10–20 cm of the ice wall, and a turbulent flow up the remainder of the ice wall (figure 6). At the top of the tank, the cold meltwater spread out to form a layer that slowly filled the tank from above. The regular photographs and several thermistors in the tank were used to monitor the propagation of this cold water front down the tank. All our experimental results were obtained at times and heights below the position of this descending cold front, where T_f was constant to within 0.1 °C.

On the turbulent part of the wall, the position of the ice interface was measured as a function of time, for the first 2 cm of ablation. The ablation velocity V was found
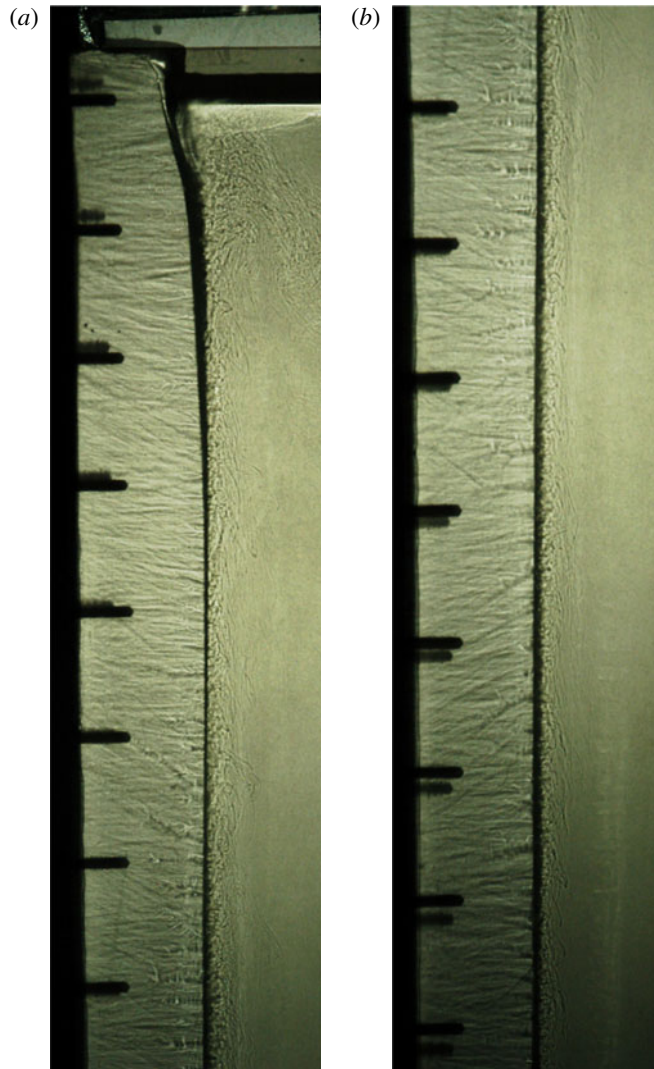
FIGURE 6. (Colour online) Shadowgraph of the turbulent compositional boundary layer flowing up the ice wall, after approximately 20 min of a qualitative experiment with $T_f = 3.9\,°C$ and $C_f = 3.31$ wt% NaCl. The vertical spacing of the black screws in the side walls is 6 cm. (*a*) The ice from a height of 72 cm up to the free surface height at 114 cm; (*b*) the ice wall at height of 32–76 cm.

to be constant with time and height, with a standard deviation of 6 %, and is listed for each experiment in table 3.

Temperatures in the ice were recorded throughout each experiment, using thermistors at heights of 32 cm, 42 cm, 56 cm and 70 cm (where two laterally displaced thermistors were placed). They showed a gradual increase in temperature with time until they reached the interface, and then a faster increase in temperature with significant fluctuations as they entered the turbulent upflow. The interface temperatures T_w were constant with time and height to within $0.1\,°C$ (table 3).
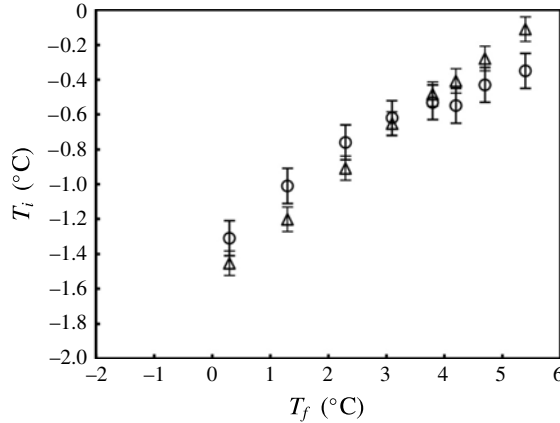
FIGURE 7. A comparison of the predicted interface temperature T_i ($\triangle$) with the interface temperature T_w ($\bigcirc$) measured in our experiments, plotted as a function of the temperature T_f of the NaCl solution. The experiments vary in C_f from 3.44 to 3.60 wt% NaCl, and in $T_i - T_s$ from 24 °C to 4 °C. The error bar of 0.07 °C in T_i results from the combined errors in D, T_f, V and $\mathrm{d}T/\mathrm{d}t$.

Although the ice block used in our experiments is much thinner than h_s, the measured temperature rise $\mathrm{d}T/\mathrm{d}t$ in the ice near the interface can be used to evaluate the equivalent temperature difference $T_i - T_s$ of a semi-infinite block of ice:

$$T_i - T_s = \frac{\mathrm{d}T}{\mathrm{d}t} \frac{\kappa_s}{V^2}, \tag{3.2}$$

which was obtained from (2.6). The values of $T_i - T_s$ are listed for each experiment in table 3. The values of $\mathrm{d}T/\mathrm{d}t$ are accurate to approximately 20 %, which translates into error bars of approximately 40 % in $T_i - T_s$, 0.04 °C in T_i and 2–4 % in $\mathcal{V}$.

In figure 7, the measured interface temperatures T_w are compared with interface temperatures T_i predicted by the turbulent dissolution model using (2.5) and (2.24). T_w and T_i are found to mostly agree to within approximately 0.2 °C. However, the transition from dissolving to melting is seen in experiments E–H, as T_w steadily departs from T_i. This result is anticipated, as (2.24) is only expected to be accurate for $\mathcal{C} \sim 1$ or greater, while $\mathcal{C}$ decreases from 0.31 in experiment E down to 0.06 in experiment H. In experiment H, the 0.24 °C difference between T_i and T_w leads to a 4 % underestimate in $\mathcal{V}$.

In figure 8, the experimental dissolving velocities V are plotted against the predicted velocity scale $\mathcal{V}$ from (3.1). The dissolving velocities are seen to lie on a straight line, with slope $\gamma = 0.090 \pm 0.004$. This result is in good agreement with the slope $\gamma = 0.093 \pm 0.010$ seen in figure 3 for the experiments of Josberger & Martin (1981), and with the value $\gamma = 0.097 \pm 0.010$ predicted from the turbulent heat transfer expressions (2.1) and (2.3) in §2.1.

4. Ice dissolution in seawater

Like the predictions for the experiments with aqueous NaCl solutions in tables 2 and 3, the model in §2.2 can be used to quantify the dissolution by turbulent compositional convection of a vertical ice surface in seawater. The ice is assumed to
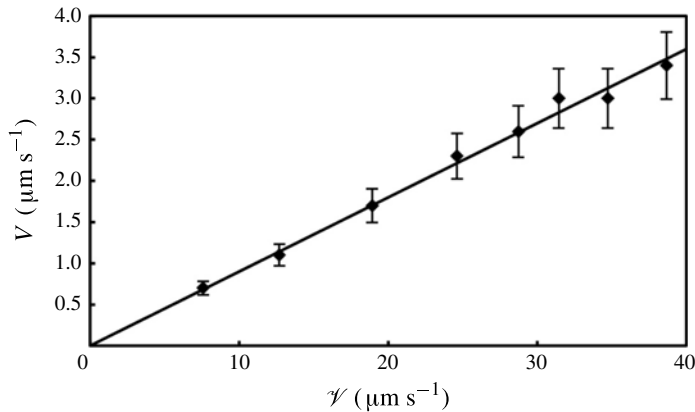
FIGURE 8. The dissolving velocities V (in μm s^{-1}) of our ice ablation experiments, in comparison with the velocity scale $\mathscr{V}$ defined by (3.1). The error bars in V show two standard deviations ($\pm 12\,\%$). The values lie on a straight line with a constant of proportionality of 0.090 ± 0.004.

have an interior temperature of $-17\,°$C (Diemand 1984), and the ocean is assumed to have a salinity C_f of 34 PSU and a corresponding surface freezing point of $T_L(C_f) = -1.86\,°$C. Its density, specific heat and freezing point are obtained from an online calculator (see http://fermi.jhuapl.edu/denscalc.html) of the UNESCO International Equation of State (UNESCO 1981), while its thermal conductivity and viscosity are obtained from tabulations (see http://web.mit.edu/seawater/) of the correlations of Sharqawy, Lienhard V & Zubair (2010). For D, the compositional diffusivity of NaCl is used (see table 2). The constant γ is taken to be 0.092, which is about the average of the experimental values of γ found in figures 5 and 8.

The dissolution calculations are summarized in table 4, for increments in T_f of $0.5\,°$C, until the dissolving model breaks down (i.e. $\mathscr{C} = 0$) at an ocean temperature T_f of $5.9\,°$C. The interface temperature T_i (in $°$C) and and interface concentration C_i (in PSU) are plotted in figures 9 and 10. Both T_i and C_i are almost linearly dependent on T_f, and can be accurately fitted by the quadratic expressions

$$T_i = T_L(C_f) + 0.251\,T_d - 0.0013\,T_d^2 \tag{4.1}$$

and

$$C_i = C_f - 4.46\,T_d + 0.0096\,T_d^2, \tag{4.2}$$

where the driving temperature difference $T_d = T_f - T_L(C_f)$ is in K. Figure 4 suggests that (4.1) is accurate to within $0.1\,°$C for T_f up to approximately 3–4 $°$C, while figure 7 indicates that (4.1) slightly overestimates the interface temperature at higher ocean temperatures, as the transition from turbulent dissolving to turbulent melting is approached.

The calculated dissolving velocities V in table 4 are shown as a function of ocean temperature as the solid line in figure 11. In terms of the driving temperature difference T_d, V can be accurately fitted by the power-law expression

$$V = 7.8\,T_d^{1.34}. \tag{4.3}$$
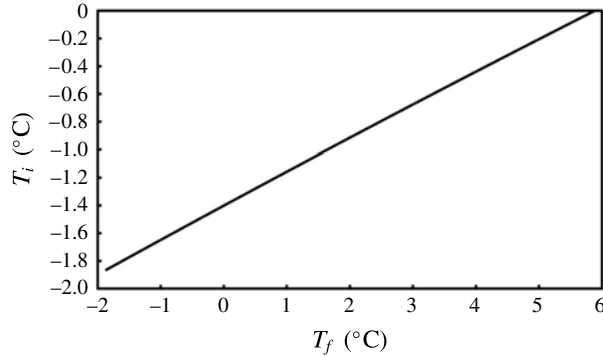
FIGURE 9. Interface temperature T_i as a function of the ocean temperature T_f, from the dissolution calculations in table 4.

T_f (°C)	C_i (PSU)	T_i (°C)	$\mathscr{C}$	V (m yr^{-1})	h_s (m)
−1.5	32.4	−1.77	19.9	2.02	18.8
−1.0	30.2	−1.65	7.8	6.41	5.92
−0.5	27.9	−1.52	4.6	11.8	3.21
0.0	25.7	−1.40	3.1	17.9	2.11
0.5	23.5	−1.28	2.2	24.6	1.54
1.0	21.3	−1.16	1.7	31.9	1.19
1.5	19.1	−1.04	1.3	39.6	0.96
2.0	16.9	−0.92	0.99	47.7	0.79
2.5	14.7	−0.80	0.76	56.2	0.67
3.0	12.5	−0.68	0.58	65.1	0.58
3.5	10.3	−0.56	0.44	74.3	0.51
4.0	8.2	−0.44	0.32	83.9	0.45
4.5	6.0	−0.32	0.21	93.7	0.40
5.0	3.8	−0.21	0.13	104	0.36
5.5	1.7	−0.09	0.051	114	0.33

TABLE 4. The dissolution by turbulent compositional convection of a vertical ice surface in a polar ocean. The ocean has a salinity of 34 PSU, and the ice has an interior temperature of −17 °C (Diemand 1984). The ice parameters used are $\rho_s L_s = 306$ J cm^{-3} (Washburn 1926), $\rho_s c_s = 1.832$ J cm^{-3} K^{-1} (Weast 1989) and $k_s = 0.022$ W cm^{-1} K^{-1} (Washburn 1926; Kaye & Laby 1973).

This result shows that the predicted dissolving velocity is very close to a 4/3 power law dependence on T_d, which arises because both $\rho_f - \rho_i$ and $C_f - C_i$ in (2.23) are almost linearly dependent on T_d. Equation (4.3) can be contrasted with an array of empirical fits and models for the ablation of ice in the ocean, which have suggested that the dependence of V on T_d might be linear (Budd *et al.* 1980; Rignot & Jacobs 2002; Shepherd *et al.* 2004), or a 3/2 power law (Russell-Head 1980), or a 8/5 power law (Greisman 1979; Josberger & Martin 1981; Neshyba & Josberger 1980), or a quadratic (Macayeal 1984; Holland, Jenkins & Holland 2008).

The calculated dissolving velocities in table 4 can be compared with a number of field observations. First, Neshyba & Josberger (1980) report an ablation velocity of
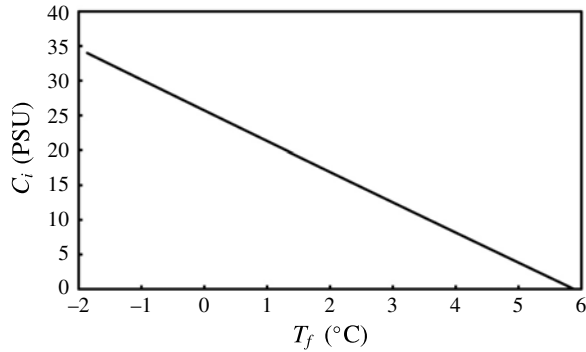
FIGURE 10. Interface concentration C_i as a function of the ocean temperature T_f, from the dissolution calculations in table 4.
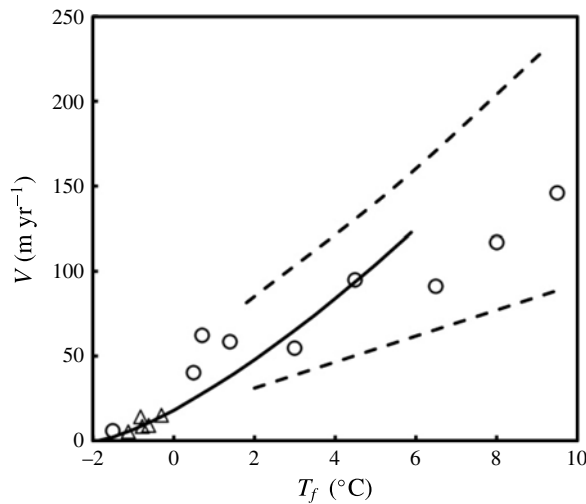
FIGURE 11. Dissolving velocity V as a function of the ocean temperature T_f, from the calculations in table 4 (solid line). The triangles show the basal ablation velocities of five West Antarctic ice shelves in the Amundsen Sea between 1992 and 2001, measured by satellite radar interferometry (Shepherd *et al.* 2004). The circles show estimates of the ablation velocities of the sides of Antarctic icebergs, while the dashed curves indicate upper and lower bounds on these estimates (Budd *et al.* 1980).

$\sim$2 m yr^{-1} in $-1.5\,^\circ$C water for an iceberg frozen fast in pack ice in d'Iberville Fjord, Northwest Territories, Canada, which was 'free of wave erosion and associated calving'. This observation is consistent with the dissolving velocity of 2.02 m yr^{-1} at $-1.5\,^\circ$C listed in table 4. Second, Budd *et al.* (1980) estimated the ablation velocities of the sides of Antarctic icebergs, by combining observations as a function of latitude of their size distribution, their drift rate, and the mean ocean temperature in the upper 200 m. These ablation velocities are plotted as circles on figure 11, together with dashed curves showing upper and lower bounds, and they are seen to be reasonably consistent with the solid line that shows the dissolving velocity calculations in table 4. Third, Shepherd *et al.* (2004) used satellite radar interferometry to measure the basal ablation velocities of five West Antarctic ice shelves in the Amundsen Sea between

1992 and 2001. Their ablation velocities are plotted as triangles on figure 11, where they are seen to be reasonably consistent with the dissolving velocity calculations in table 4, although we caution that ice shelves have complex ice interface geometries (e.g. Rignot & Steffen 2008; Vaughan *et al.* 2012; Dutrieux *et al.* 2014), and they can be affected by ocean stratification and ambient currents in particular locations.

5. Conclusions

In this paper, we have examined the dissolution driven by turbulent compositional convection of a vertical solid surface in contact with a solution whose composition is different to that of the solid. Guided by experimental measurements for turbulent natural convection on a vertical boundary, we developed a theoretical model that has no free parameters and no dependence on height. The model predicts the interface concentration from (2.24), the interface temperature from (2.5), and the dissolving velocity from (2.23).

We have compared our model with laboratory experiments, made by both Josberger & Martin (1981) and ourselves, in which vertical ice walls were dissolved in contact with aqueous NaCl solutions. In the experiments, the interface temperatures and dissolution velocities are observed to be independent of height. We find that the model predicts the measured dissolving velocities to within 10 %, for water temperatures up to approximately 5–6 °C (where there is a transition from turbulent dissolution to turbulent melting). In § 4, we take an ocean of salinity 34 PSU and evaluate the dissolution by turbulent compositional convection of a vertical ice body with an interior temperature of -17 °C. We find that the dissolution velocity depends on the 4/3 power of the difference between the ocean temperature and its freezing point, and that it is reasonably consistent with some observations of the ablation velocities of icebergs and ice shelves (figure 11).

We also note that scaling theory for both horizontal and vertical boundaries suggests that a second regime of turbulent natural convection may exist at high enough Rayleigh numbers, where the thickness of the inner laminar boundary layer near the wall is controlled by shear instability rather than convective instability (e.g. Grossmann & Lohse 2000; Wells & Worster 2008). The transition is predicted to occur at $Ra \sim 10^{16}$ for thermal convection in air (where the Prandtl number $Pr = \nu/\kappa \approx 0.7$). However, for compositional convection during ice dissolution (where the Schmidt number $Sc = \nu/D \approx 2600$), the transition is predicted to occur at $Ra \sim 10^{21}$ (cf. figure 2 of Grossmann & Lohse 2000), which would require vertical ice heights H of hundreds of metres. It would be interesting to undertake careful quantitative observations on the sides of large tabular Antarctic icebergs for comparison with these convective scaling theories.

Acknowledgements

REFERENCES

BATCHELOR, G. K. 1967 *An Introduction to Fluid Dynamics*. Cambridge University Press.
BUDD, W. F., JACKA, T. H. & MORGAN, V. I. 1980 Antarctic iceberg melt rates derived from size distributions and movement rates. *Ann. Glaciol.* **1**, 103–112.

CAREY, V. P. & GEBHART, B. 1982 Transport near a vertical ice surface melting in saline water: experiments at low salinities. *J. Fluid Mech.* **117**, 403–423.

CARSLAW, H. S. & JAEGER, J. C. 1986 *Conduction of Heat in Solids*. Oxford University Press.

DIEMAND, D. 1984 Iceberg temperatures in the North Atlantic – theoretical and measured. *Cold Reg. Sci. Technol.* **9**, 171–178.

DUTRIEUX, P., STEWART, C., JENKINS, A., NICHOLLS, K. W., CORR, H. F. J., RIGNOT, E. & STEFFAN, K. 2014 Basal terraces on melting ice shelves. *Geophys. Res. Lett.* **41**, doi:10.1002/2014GL060618.

GREISMAN, P. 1979 On upwelling driven by the melt of ice shelves and tidal glaciers. *Deep-Sea Res.* **26A**, 1051–1065.

GROSSMANN, S. & LOHSE, D. 2000 Scaling in thermal convection: a unifying theory. *J. Fluid Mech.* **407**, 27–56.

HOLLAND, P. R., JENKINS, A. & HOLLAND, D. M. 2008 The response of ice shelf basal melting to variations in ocean temperature. *J. Clim.* **21**, 2558–2572.

HOLMAN, J. P. 2010 *Heat Transfer*, 10th edn. McGraw-Hill.

HOWARD, L. N. 1966 Convection at high Reynolds number. In *Proceedings of the 11th International Congress of Applied Mechanics, Munich* (ed. H. Görtler), pp. 1109–1115. Springer.

JENKINS, A., DUTRIEUX, P., JACOBS, S. S., MCPHAIL, S. D., PERRETT, J. R., WEBB, A. T. & WHITE, D. 2010 Observations beneath Pine Island Glacier in West Antarctica and implications for its retreat. *Nat. Geosci.* **3**, 468–472.

JOHNSON, R. S. & MOLLENDORF, J. C. 1984 Transport from a vertical ice surface in saline water. *Intl J. Heat Mass Transfer* **27**, 1928–1932.

JOSBERGER, E. G. 1979 Laminar and turbulent boundary layers adjacent to melting vertical ice walls in salt water. PhD thesis, University of Washington, Seattle.

JOSBERGER, E. G. & MARTIN, S. 1981 A laboratory and theoretical study of the boundary layer adjacent to a vertical melting ice wall in salt water. *J. Fluid Mech.* **111**, 439–473.

KATSAROS, K. B., LIU, W. T., BUSINGER, J. A. & TILLMAN, J. E. 1977 Heat transport and thermal structure in the interfacial boundary layer measured in an open tank of water in turbulent free convection. *J. Fluid Mech.* **83**, 311–335.

KAYE, G. W. C. & LABY, T. H. 1973 *Tables of Physical and Chemical Constants and some Mathematical Functions*. Longman.

KERR, R. C. 1994a Melting driven by vigorous compositional convection. *J. Fluid Mech.* **280**, 255–285.

KERR, R. C. 1994b Dissolving driven by vigorous compositional convection. *J. Fluid Mech.* **280**, 287–302.

LICK, W. 1965 The instability of a fluid layer with time-dependent heating. *J. Fluid Mech.* **21**, 565–576.

MACAYEAL, D. R. 1984 Thermohaline circulation below the Ross Ice Shelf: a consequence of tidally induced vertical mixing and basal melting. *J. Geophys. Res.* **89**, 597–606.

NESHYBA, S. & JOSBERGER, E. G. 1980 On the estimation of Antarctic iceberg melt rate. *J. Phys. Oceanogr.* **10**, 1681–1685.

RIGNOT, E. & JACOBS, S. S. 2002 Rapid bottom melting widespread near Antarctic ice sheet grounding lines. *Science* **296**, 2020–2023.

RIGNOT, E., JACOBS, S., MOUGINOT, J. & SCHEUCHL, B. 2013 Ice shelf melting around Antarctica. *Science* **341**, 266–270.

RIGNOT, E. & STEFFEN, K. 2008 Channelized bottom melting and stability of floating ice shelves. *Geophys. Res. Lett.* **35**, L02503.

RIGNOT, E., VELICOGNA, I., VAN DEN BROEKE, M. R., MONAGHAN, A. & LENAERTS, J. 2011 Acceleration of the contribution of the Greenland and Antarctic ice sheets to sea level rise. *Geophys. Res. Lett.* **38**, L05503.

RUSSELL-HEAD, D. S. 1980 The melting of free-drifting icebergs. *J. Glaciol.* **1**, 119–121.

SHARQAWY, M. H., LIENHARD V, J. H. & ZUBAIR, S. M. 2010 Thermophysical properties of seawater: a review of existing correlations and data. *Desalin. Water Treat.* **16**, 354–380.

SHEPHERD, A., WINGHAM, D. & RIGNOT, E. 2004 Warm ocean is eroding West Antarctic Ice Sheet. *Geophys. Res. Lett.* **31**, L23402.

TURNER, J. S. 1979 *Buoyancy Effects in Fluids*. Cambridge University Press.

UNESCO 1981 Background papers and supporting data on the International Equation of State of Seawater 1980. *UNESCO Technical Papers in Marine Science* No. 38.

VAUGHAN, D. G., CORR, H. F. J., BINDSCHADLER, R. A., DUTRIEUX, P., GUDMUNDSSON, G. H., JENKINS, A., NEWTON, T., VORNBERGER, P. & WINGHAM, D. J. 2012 Subglacial melt channels and fracture in the floating part of Pine Island Glacier, Antarctica. *J. Geophys. Res.* **117**, F03012.

VLIET, G. C. & ROSS, D. C. 1975 Turbulent natural convection on upward and downward facing inclined constant heat flux surfaces. *Trans. ASME: J. Heat Transfer* **97**, 549–555.

WARNER, C. Y. & ARPACI, V. S. 1968 An experimental investigation of turbulent natural convection in air at low pressure along a vertical heated flat plate. *Intl J. Heat Mass Transfer* **11**, 397–406.

WASHBURN, E. W. (Ed.) 1926 *International Critical Tables of Numerical Data: Physics, Chemistry and Technology*. National Academic Press.

WEAST, R. C. (Ed.) 1989 *CRC Handbook of Chemistry and Physics*. CRC Press.

WELLS, A. J. & WORSTER, M. G. 2008 A geophysical-scale model of vertical natural convection boundary layers. *J. Fluid Mech.* **609**, 111–137.

WELLS, A. J. & WORSTER, M. G. 2011 Melting and dissolving of a vertical solid surface with laminar compositional convection. *J. Fluid Mech.* **687**, 118–140.

WOODS, A. W. 1992 Melting and dissolving. *J. Fluid Mech.* **239**, 429–448.